Clinical and Experimental Medicine (2025) 25:67
https://doi.org/10.1007/s10238-025-01593-3

RESEARCH

Activation of RHO-GTPase gene pattern correlates with adverse clinical outcome and immune microenvironment in clear cell renal cell carcinoma

Kehang Guo[1,2] · Pengyue Ma[3] · Qi Yang[2] · Lingli Xu[4] · Biixiong Zhang[2] · Hong Zhang[5] · Zhongwen Zheng[2,6] · Zewei Zhuo[2,7]

Received: 11 January 2025 / Accepted: 8 February 2025

Abstract

Clear cell renal cell carcinoma (ccRCC), the most prevalent renal cancer subtype, is frequently associated with poor prognosis. RHO-GTPase signaling genes have been implicated in tumor aggressiveness and unfavorable survival, but their potential in risk stratification and therapeutic guidance for ccRCC patients remains unexplored. Univariate regression identified prognostically relevant RHO-GTPase signaling genes, followed by consensus clustering for ccRCC subtype classification. LASSO regression selected key genes to construct a six-gene risk model. The model was evaluated for prognostic stratification, immune status, immunotherapy response, and chemotherapy sensitivity. Key genes were analyzed at the genomic, single-cell, and protein levels to explore underlying mechanisms. Among 62 prognostically relevant RHO-GTPase signaling genes, six (ARHGAP11B, NUF2, PLK1, CYFIP2, IQGAP2, and VAV3) were identified to form a robust prognostic signature. This model stratified patients into high- and low-risk groups, with high-risk patients demonstrating significantly worse outcomes. The model exhibited excellent predictive accuracy (AUC > 0.7 in training and validation cohorts). High-risk patients were characterized by an immunosuppressive microenvironment and reduced sensitivity to immunotherapy. Drug sensitivity analysis revealed 107 agents correlated with the risk score, underscoring therapeutic relevance. Mechanistically, the six key genes showed distinct expression patterns, cellular distribution, and positive correlation with VHL mutations, highlighting their potential as actionable drug targets. This study established a novel six-gene RHO-GTPase signaling model for predicting prognosis, immune status, and therapeutic responses in ccRCC, which offers potential for improving patient stratification and guiding personalized treatment strategies.

Keywords RHO-GTPase · Single-cell · Immune microenvironment · Drug response · Clear cell renal cell carcinoma

Kehang Guo, Pengyue Ma, and Qi Yang have contributed equally to this work.

✉ Hong Zhang
zhanghong4809@gdph.org.cn

✉ Zhongwen Zheng
zhengzhongwen@gdph.org.cn

✉ Zewei Zhuo
zhuozewei@gdph.org.cn

[1] Department of Critical Care Medicine, The Fifth Affiliated Hospital of Zhengzhou University, Zhengzhou 450000, China

[2] Department of Gastroenterology, Guangdong Provincial People's Hospital (Guangdong Academy of Medical Sciences), Southern Medical University, Guangzhou 510080, China

[3] Department of Nephrology, The Second Affiliated Hospital of Zhengzhou University, Zhengzhou, China

[4] Dadong Street Community Health Service Center, Guangzhou 510080, China

[5] Department of Lymphoma, Guangdong Provincial People's Hospital, Guangdong Academy of Medical Sciences, Southern Medical University, Guangzhou 510080, China

[6] Heyuan People's Hospital, Heyuan 517001, Guangdong, China

[7] School of Medicine, South China University of Technology, Guangzhou 510006, China

Published online: 25 February 2025

Introduction

Clear cell renal cell carcinoma (ccRCC) is a prevalent form of renal malignancy characterized by poor prognosis and limited treatment options [1]. Despite recent advancements in targeted therapies and immunotherapy, the overall survival rate for patients with advanced ccRCC remains low [2]. The unique biological features of ccRCC render it highly resistant to conventional chemotherapy and radiotherapy, making surgical intervention the primary treatment for localized disease [3, 4]. However, for metastatic ccRCC, the emergence of resistance and limited long-term efficacy of targeted therapies and immune checkpoint inhibitors continue to pose significant clinical challenges [5, 6]. Moreover, studies indicate that the molecular heterogeneity of ccRCC and the presence of diverse biomarkers significantly influence treatment responses, further complicating therapeutic approaches [7, 8]. Consequently, identifying novel biomarkers to enhance prognostic accuracy and guide personalized treatment strategies has become a pivotal focus of current research [9].

RHO-GTPases, a family of small GTP-binding proteins, play essential roles in various cellular processes, including cytoskeletal remodeling, cell migration, and intracellular signaling [10]. In the context of ccRCC, RHO-GTPases are increasingly recognized for their involvement in tumor progression and metastasis. Specifically, proteins such as RhoA, Rac1, and Cdc42 regulate the invasive and migratory abilities of ccRCC cells, key processes underlying cancer metastasis [11]. Furthermore, the RHO-GTPase signaling pathway interacts with the hypoxia-inducible factor (HIF) pathway, which is frequently dysregulated in ccRCC due to VHL gene inactivation [12, 13]. This intricate crosstalk highlights the multifaceted roles of RHO-GTPases in ccRCC and their potential as biomarkers for disease progression and therapeutic targets.

Given their critical role in ccRCC, RHO-GTPases offer promising potential for improving prognostic models and personalized therapies. In this study, we aim to develop a prognostic model based on RHO-GTPase genes to assess outcomes and guide treatment. Using machine learning, we identified key feature genes and created an RHO-GTPase risk score to stratify patients by risk level, providing insights into prognosis, immune status, immunotherapy response, and chemotherapy sensitivity. Additionally, we analyzed RHO-GTPase gene distribution at transcriptomic and single-cell levels, creating a comprehensive clinical nomogram. This integrative analysis offers a novel framework for personalized treatment strategies, potentially improving clinical outcomes for ccRCC patients. The study design is shown in Fig. 1A.

Methods

Data acquisition and preprocessing

RNA-sequencing data and corresponding clinical information for ccRCC patients were downloaded from The Cancer Genome Atlas (TCGA) database and Gene Expression Omnibus (GEO) (GSE29609). Tumor tissues and adjacent normal tissues were included in the analysis. RHO-GTPase family genes were extracted from molecular signatures database (MSigDB). Immunotherapeutic response data (anti-PD-1 therapy) were obtained from Braun's study [14]. A single-cell cohort of ccRCC tissues was obtained from GSE139555. Differentially expressed genes (DEGs) were identified using the threshold of $|Log2FC| > 2$ and $P\text{-value} < 0.05$. Data preprocessing and analysis were conducted using R software (v4.2.0).

Identification of prognosis-associated RHO-GTPase genes

Univariate Cox regression analysis was performed to evaluate the association of RHO-GTPase genes with overall survival (OS). Genes with a $P\text{-value} < 0.05$ were considered significant. The intersection of the DEGs and prognosis-related genes was taken, identifying prognostic DEGs using Venn diagrams. Visualization of DEGs was achieved using volcano plots. Protein–protein interaction (PPI) networks were constructed using STRING database.

Consensus clustering for patient subtyping

Consensus clustering was conducted to classify ccRCC patients into molecular subtypes based on the expression of the prognosis-related RHO-GTPase genes. The ConsensusClusterPlus package in R was utilized, with the cumulative distribution function (CDF) and delta area curves determining the optimal number of clusters. Principal component analysis (PCA) and heatmaps were employed to validate the clustering results and visualize gene expression patterns across the subtypes. Kaplan–Meier survival analysis was performed to evaluate survival differences among clusters.

Differential expression and functional enrichment analysis

To investigate biological differences between clusters, differential expression analysis was conducted between Cluster 1 and Cluster 2 using the "Limma" package in R. Genes with $|Log2FC| > 1$ and adjusted $P\text{-value} < 0.05$ were considered significant. Gene Ontology (GO) and Kyoto Encyclopedia of

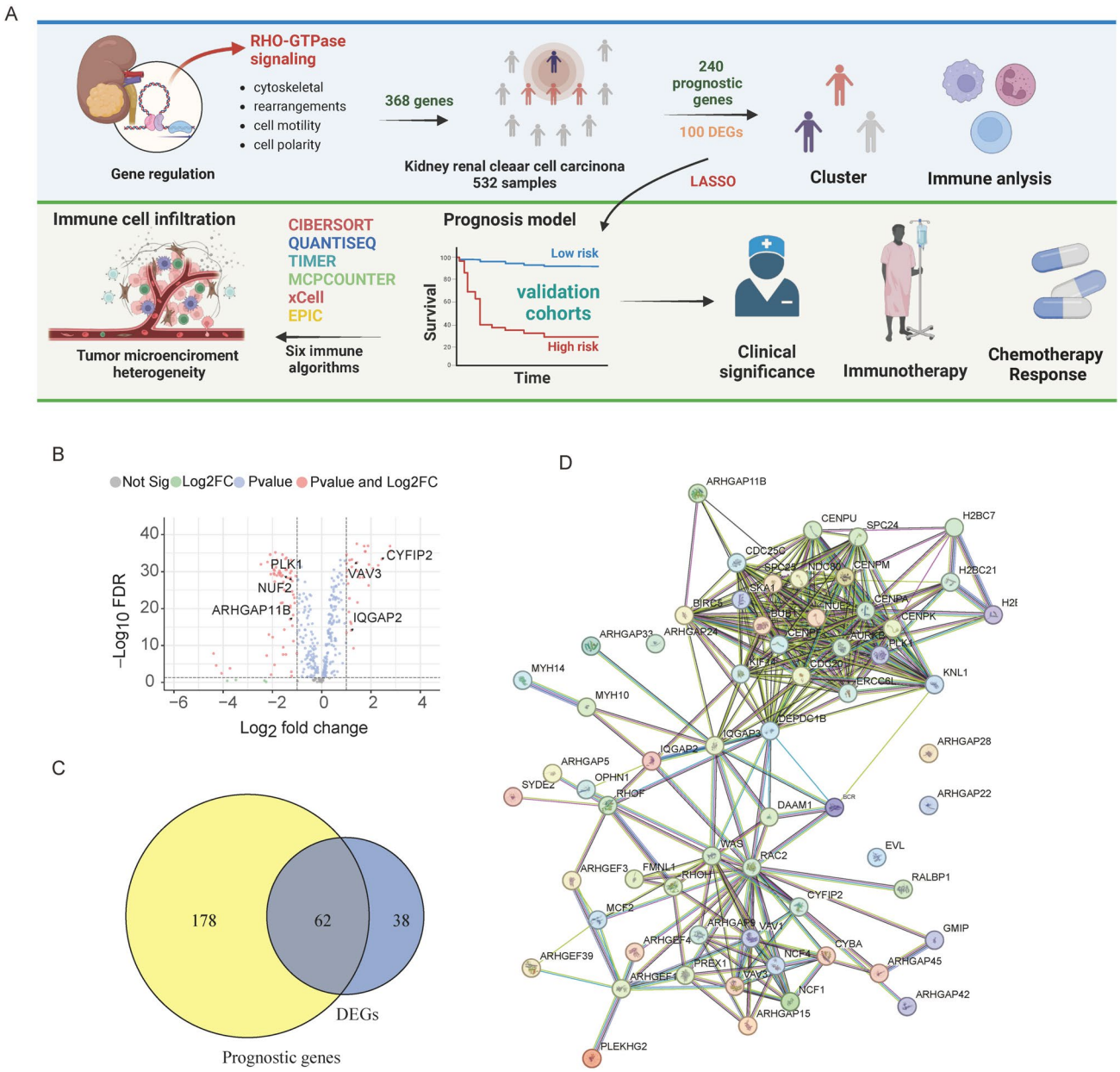

Fig. 1 mRNA expression and survival relevance of RHO-GTPase genes in ccRCC patients. **A** Study overview. **B** Volcano plot of RHO-GTPase gene expression. **C** Venn diagram showing the overlap of differentially expressed and prognostic RHO-GTPase genes, resulting in 62 prognostic genes. **D** Protein–protein interaction network of the 62 prognostic RHO-GTPase genes

Genes and Genomes (KEGG) pathway enrichment analyses were performed on upregulated and downregulated genes using the "clusterProfiler" package.

Immune microenvironment analysis

The CIBERSORT algorithm was employed to quantify the infiltration of 22 immune cell types across the three clusters. Differential immune cell infiltration was compared using the Wilcoxon rank-sum test. Additionally, the expression of immune checkpoint-related genes (e.g., CD274, CTLA4, HAVCR2, IGSF8, ITPRIPL1, LAG3, PDCD1, PDCD1, LG2, SIGLEC15, and TIGIT) was analyzed across clusters to elucidate immune suppression mechanisms.

Construction and validation of prognostic models

LASSO Cox regression analysis was applied to refine the prognostic RHO-GTPase DEGs into a gene signature predictive of patient survival. The predictive accuracy of the

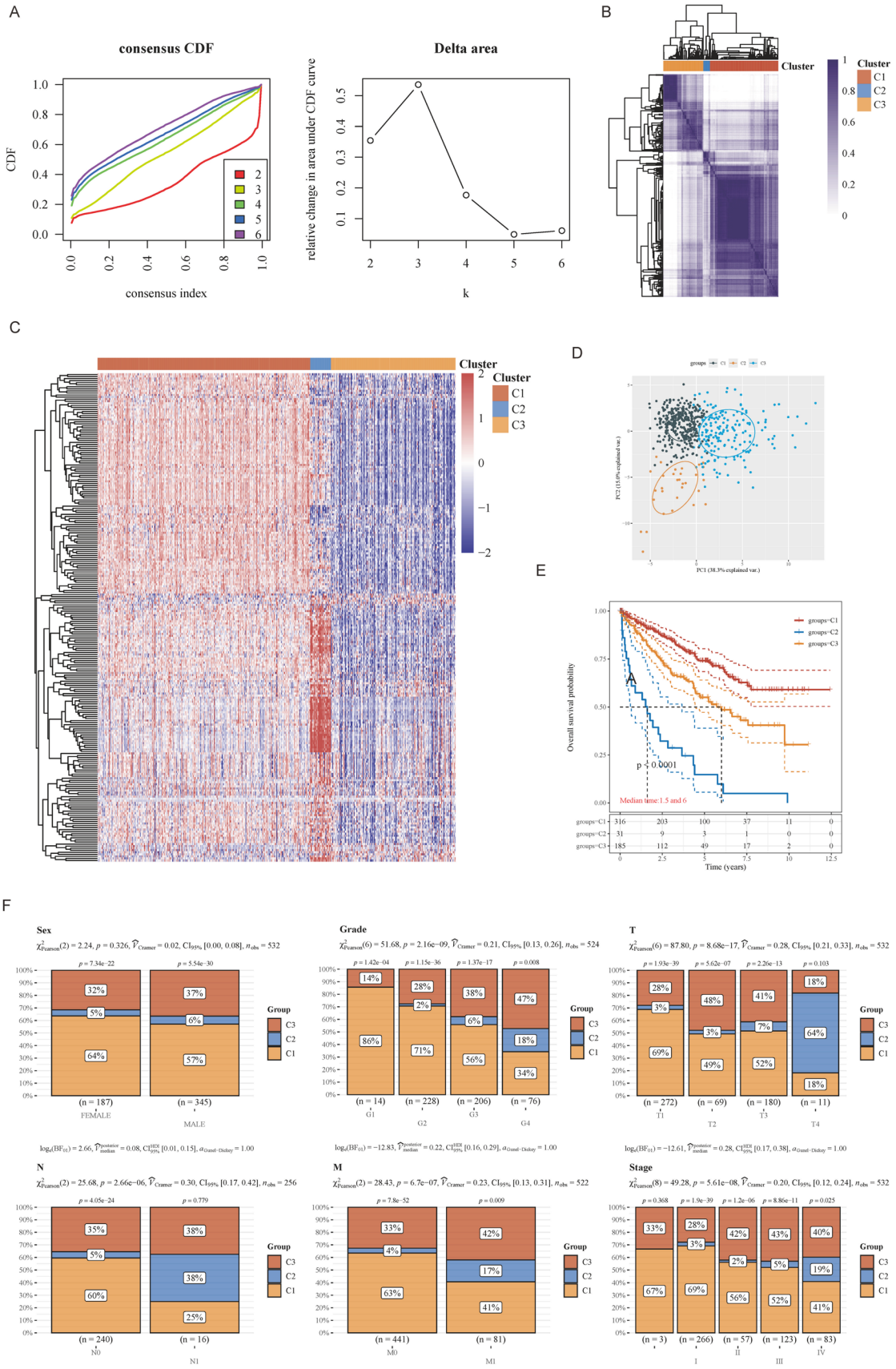
A
consensus CDF
CDF
consensus index
Delta area
relative change in area under CDF curve
k
B
Cluster
C1
C2
C3
C
Cluster
D
groups
PC1 (38.3% explained var.)
PC2 (18.0% explained var.)
E
Overall survival probability
p = 0.0001
Median time:1.5 and 6
groups=C1
groups=C2
groups=C3
Time (years)
F
Sex
Grade
T
N
M
Stage
Group
FEMALE
MALE
G1
G2
G3
G4
T1
T2
T3
T4
N0
N1
M0
M1
I
II
III
IV

◂**Fig. 2** Subgroup classification of ccRCC patients based on RHO-GTPase genes. **A** CDF curve and CDF delta area curve showing the maximal area under the curve at $K=3$. **B** Consistency clustering heatmap at $K=3$ using ConsensusClusterPlus, where rows and columns represent samples, and different colors represent different clusters. **C** Gene expression heatmap of RHO-GTPase-related genes across subgroups, with red indicating high expression and blue indicating low expression. **D** Principal component analysis showing that RHO-GTPase genes can effectively distinguish the three ccRCC patient subgroups. **E** Kaplan–Meier survival curves for different subgroups. **F** Distribution of clinical features across subgroups. The x-axis represents different clinical features, and the y-axis shows the percentage of samples with the corresponding feature in each subgroup. Significance was determined using chi-square tests

model was validated in independent datasets using cross-validation techniques. Risk scores were calculated for each patient based on the gene signature, as follows:

$$\text{Rho GTPase risk score} = \sum_{i=1}^{n} Xi \times Yi$$

According to the medium risk score, ccRCC patients were stratified into high- and low-risk groups. Kaplan–Meier survival curves were used for survival analysis. Model performance was evaluated using receiver operating characteristic (ROC) curves. ccRCC patients from GSE29609 was used as validation cohort.

Immune infiltration estimations

To perform reliable immunity scoring assessments, immune cell scoring data for ccRCC patients were downloaded from the TIMER database (http://timer.cistrome.org/). This tool employs six deconvolution algorithms (TIMER, CIBERSORT, quanTIseq, xCell, MCP-counter, and EPIC) to infer immune infiltration from gene expression profiles of TCGA samples. Spearman correlation was used to analyze the relationship between risk scores and immune cell infiltration, and the results were visualized using bubble plots. Additionally, the R package "ggpubr" was used to create boxplots comparing immune cell differences between high- and low-risk groups.

Drug sensitivity analysis

To evaluate the therapeutic implications of the identified RHO-GTPase subtypes, drug sensitivity analysis was

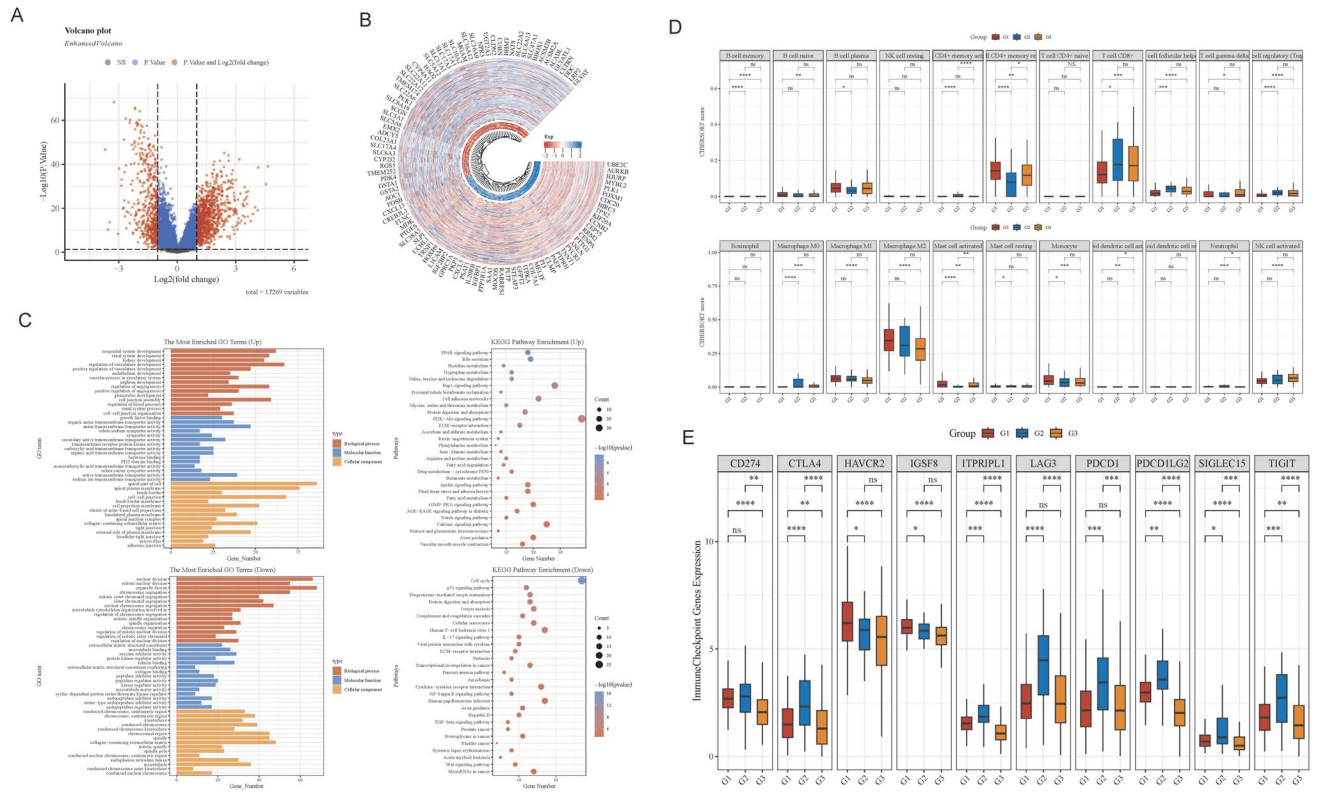

Fig. 3 Biological function analysis of ccRCC patient subgroups. **A** Volcano plot of gene expression differences between Cluster 1 and Cluster 2. **B** Expression of the top 100 differentially expressed genes (50 upregulated and 50 downregulated) between Cluster 1 and Cluster 2, showing the distribution of gene expression in the two subgroups. **C** KEGG pathway and GO term enrichment analysis of the upregulated genes in Cluster 2. **D** Immune cell infiltration levels across the three subgroups, as calculated by the CIBERSORT immune algorithm. **E** Expression of immune checkpoint genes across the three subgroups

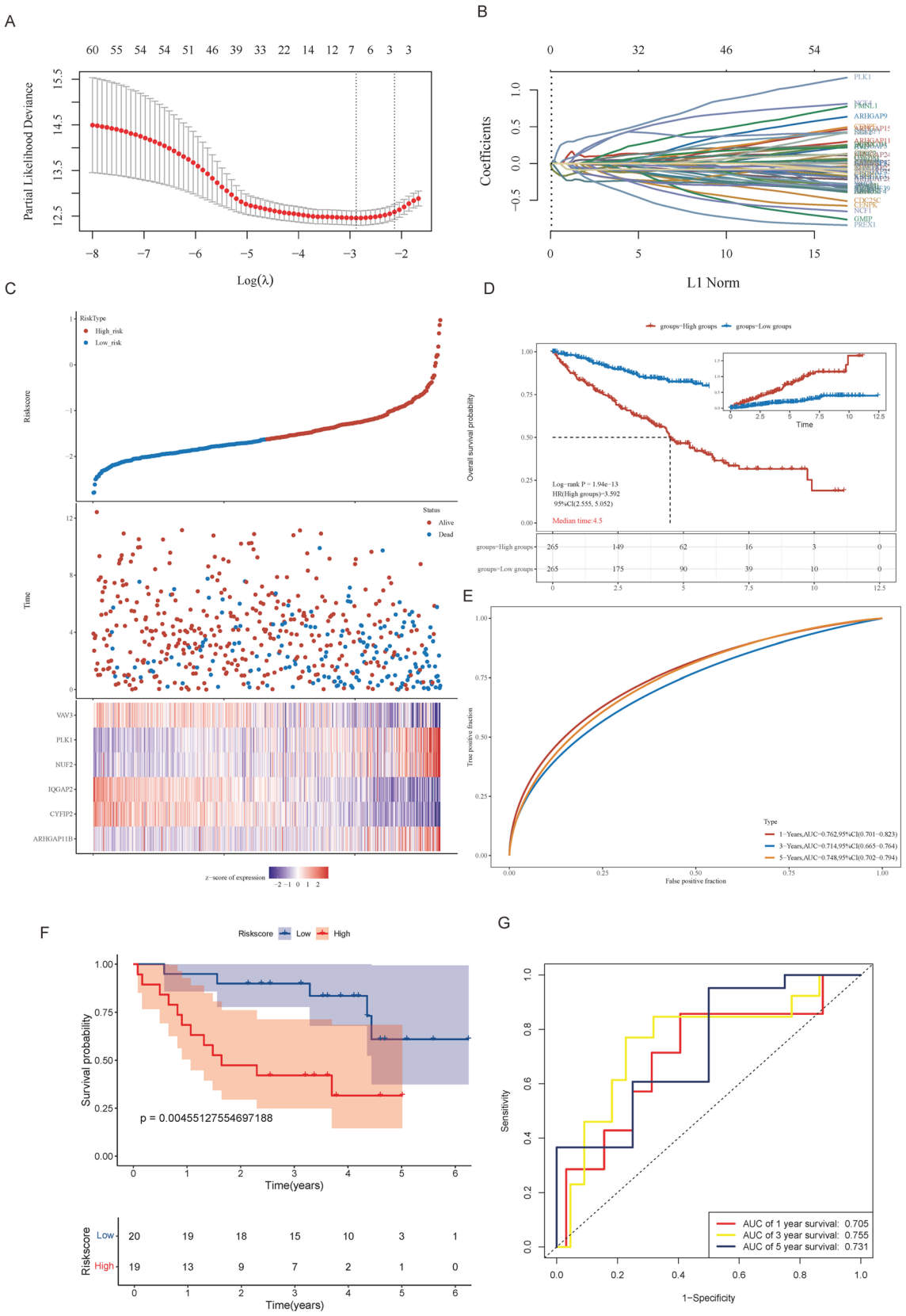
A
Partial Likelihood Deviance
Log(λ)
B
Coefficients
L1 Norm
C
RiskType
High_risk
Low_risk
Riskscore
Status
Alive
Dead
Time
VAV3
PLK1
NUF2
IQGAP2
CYFIP2
ARHGAP11B
z−score of expression
D
groups=High groups
groups=Low groups
Overall survival probability
Log−rank P = 1.94e−13
HR(High groups)=3.592
95%CI(2.555, 5.052)
Median time:4.5
E
True positive fraction
False positive fraction
Type
1−Years,AUC=0.762,95%CI(0.701−0.823)
3−Years,AUC=0.714,95%CI(0.665−0.764)
5−Years,AUC=0.748,95%CI(0.702−0.794)
F
Riskscore Low High
Survival probability
p = 0.00455127554697188
Time(years)
Low
High
G
Sensitivity
1−Specificity
AUC of 1 year survival: 0.705
AUC of 3 year survival: 0.755
AUC of 5 year survival: 0.731

◂**Fig. 4** Construction and validation of a prognostic model for ccRCC patients based on RHO-GTPase genes. **A** LASSO Cox regression model showing the relationship between the partial likelihood deviance and log(λ). **B** LASSO regression analysis identifies RHO-GTPase feature genes in ccRCC patients, with coefficients determined by the lambda parameter. **C** Distribution of RHO-GTPase risk scores, survival time, and gene expression across ccRCC patients. The top part shows the scatter plot of risk scores from low to high, with different colors representing different risk groups. The middle part shows the scatter plot distribution of risk scores, survival time, and survival status. The bottom part shows the heatmap of gene expression. **D** Kaplan–Meier survival curves for high-risk and low-risk groups. The cumulative probability curve is shown in the top right corner. **E** ROC curves for 1-year, 3-year, and 5-year survival rates in the TCGA cohort. **F** Kaplan–Meier survival curves and **G** ROC curves for the independent validation cohort (GEO)

performed using the GDSC (Genomics of Drug Sensitivity in Cancer) database. The IC50 values of chemotherapeutic agents and targeted drugs were predicted for each subtype using the "pRRophetic" R package. Comparisons of drug sensitivity between clusters were conducted using the Wilcoxon rank-sum test.

Single-cell and protein expression analysis

Single-cell RNA-sequencing data for ccRCC patients were downloaded from the GSE139555 dataset in h5 format along with the corresponding annotation results. Data were processed and analyzed using the “MAESTRO” and “Seurat” R packages. Cell clustering and grouping were reevaluated using the t-SNE method. Key gene expression patterns were further validated with immunohistochemically stained tissue section images obtained from the HPA database (https://www.proteinatlas.org/). Correlation plots between two key genes were generated using the "ggstatsplot" R package.

Statistical analysis

All statistical analyses were performed using R software. Differences between groups were assessed using the Wilcoxon rank-sum test, as appropriate. Kaplan–Meier survival curves were generated using the survminer package, and the log-rank test was used to compare survival differences. A P-value < 0.05 was considered statistically significant unless otherwise specified.

Results

Expression of RHO-GTPase genes is closely associated with survival in ccRCC patients

We obtained tumor and adjacent normal tissue samples from 530 ccRCC patients in the TCGA database. Differential gene expression analysis, using a threshold of $|Log2FC| > 2$ and P value < 0.05, identified 100 RHO-GTPase genes that were differentially expressed between ccRCC tumor tissues and adjacent normal tissues (Fig. 1B). Univariate regression analysis revealed 240 RHO-GTPase genes significantly associated with overall survival. The intersection of these two datasets yielded 62 differentially expressed RHO-GTPase genes associated with prognosis (Fig. 1C). Protein–protein interaction analysis of these 62 genes showed that NUF2, PLK1, and RAC2 were key hub genes (Fig. 1D).

RHO-GTPase genes have prognostic stratification value in ccRCC patients

Based on the 240 prognostic RHO-GTPase genes, we performed subtyping of ccRCC patients. The cumulative distribution function (CDF) and CDF delta area curves indicated that when $K = 3$, the area under the CDF curve was maximized (Fig. 2A). Consistency clustering results using ConsensusClusterPlus and principal component analysis (PCA) showed that at $K = 3$, ccRCC patients were effectively classified into three subgroups (Fig. 2B, D). Gene expression heatmap (Fig. 2C) revealed that RHO-GTPase genes were significantly underexpressed in Cluster 3, overexpressed in Cluster 2, and expressed at intermediate levels in Cluster 1. Survival analysis showed that patients with high expression of RHO-GTPase genes had the worst prognosis, while those with low or medium expression had better outcomes (Fig. 2E), suggesting that activation of RHO-GTPase genes may be associated with poorer clinical outcomes. Further analysis of clinical features showed significant associations between RHO-GTPase subgroups and tumor grade and TNM staging (Fig. 2F). As tumor grade and TNM stage progressed, the proportion of Cluster 2 increased, indicating that RHO-GTPase activation may be closely related to tumor progression.

RHO-GTPase activation is associated with an immune-suppressive microenvironment

To explore the biological differences between Cluster 1 and Cluster 2 (RHO-GTPase activation mode), we conducted a differential gene expression analysis. The volcano plot (Fig. 3A) revealed significant differentially expressed genes (DEGs) between Cluster 1 and Cluster 2, with a total of 1460 key genes identified, including 960 upregulated and 500 downregulated genes. The heatmap (Fig. 3B) showed that these genes were clearly differentiated between the two subgroups, reflecting significant biological differences. Gene Ontology (GO) analysis indicated that upregulated genes in Cluster 2 were significantly enriched in processes such as "regulation of angiogenesis," "vascular processes in the circulatory system," and "collagen-containing extracellular

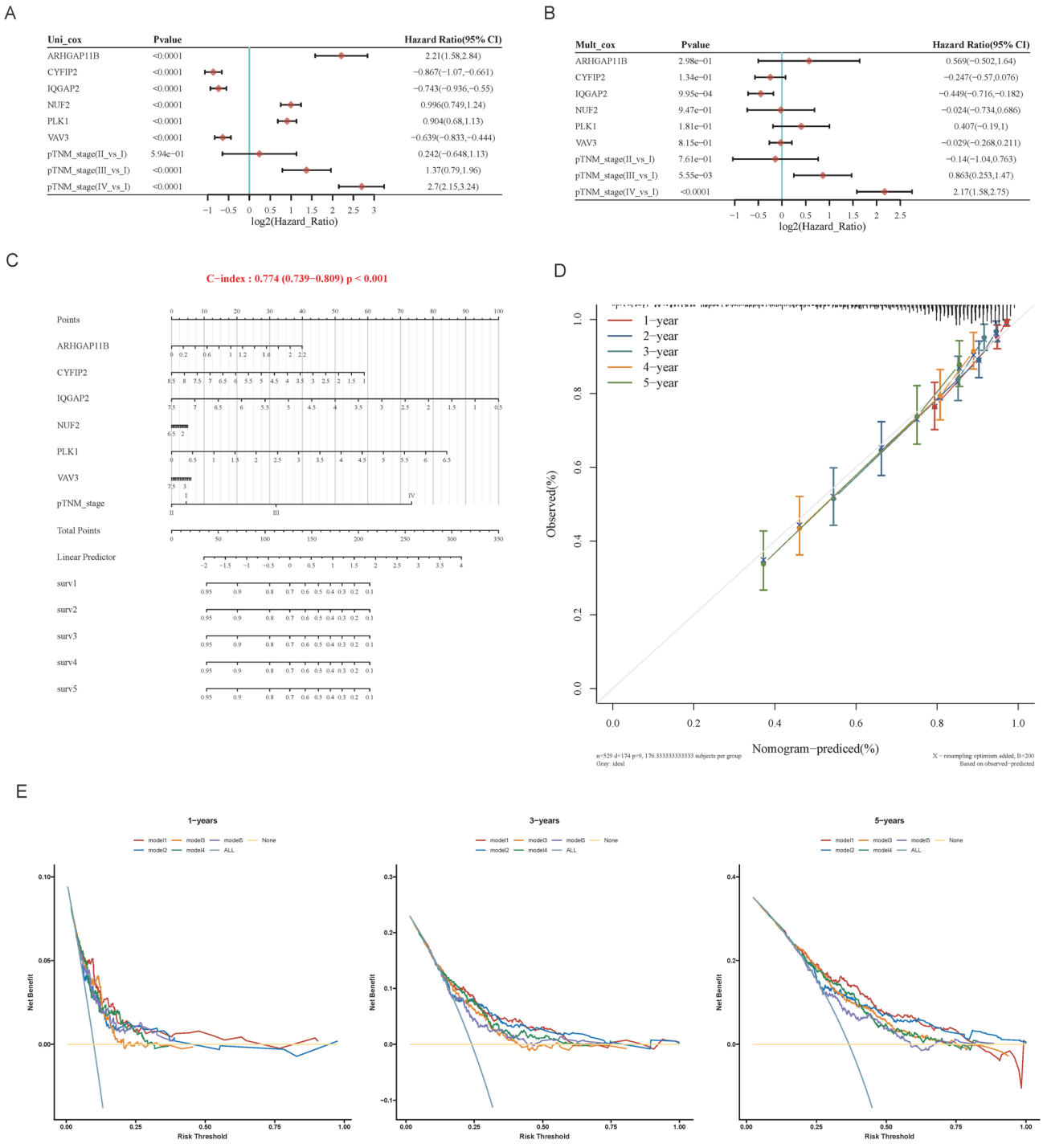

Fig. 5 Clinical nomogram for ccRCC patients based on RHO-GTPase prognostic feature genes and comparison of model performance. **A**, **B** Univariate and multivariate Cox analyses showing p-values, hazard ratios (HRs), and confidence intervals for gene expression and clinical features. **C** Clinical nomogram incorporating RHO-GTPase prognostic genes and TNM staging to predict overall survival of ccRCC patients at 1, 2, 3, 4, and 5 years, with a C-index of 0.774. **D** Calibration curve of the overall survival nomogram model, with dashed diagonal lines representing the ideal nomogram. Blue, red, and orange lines represent observed survival at 1, 2, 3, 4, and 5 years. **E** DCA (decision curve analysis) comparing the clinical utility of RHO-GTPase and other prognostic models. Model 1: RHO-GTPase-Related Prognostic Signature, Model 2: Disulfidptosis-Related Prognostic Signature, Model 3: Lactate-Related Prognostic Signature, Model 4: Hypoxia-Associated Long Noncoding RNA Signature, Model 5: Cuproptosis-Related Ferroptosis Genes. The x-axis represents threshold probability, and the y-axis represents net benefit. "None" and "ALL" refer to two reference lines. If a model's curve consistently lies above the others over a wide range of threshold probabilities, it suggests superior predictive ability

matrix," suggesting that the tumor microenvironment in Cluster 2 promotes angiogenesis and metastasis. Downregulated genes were enriched in "cell cycle regulation," "mitotic nuclear division," and "condensed chromosomal regions," indicating potential genomic regulatory abnormalities in Cluster 2. KEGG pathway analysis further revealed that upregulated genes in Cluster 2 were enriched in pathways related to angiogenesis and tumor progression, such as "vascular smooth muscle contraction," "cGMP-PKG signaling pathway," and "Notch signaling pathway." Downregulated genes were closely associated with immune response pathways, including "IL-17 signaling pathway," "NF-kappa B signaling pathway," and "cytokine–cytokine receptor interaction," suggesting significant immune suppression in Cluster 2. Using the CIBERSORT immune algorithm (Fig. 3D), we further confirmed the immune microenvironment differences between subgroups. Results showed that immune-suppressive cells, such as regulatory T cells, were significantly more infiltrated in Cluster 2 compared to Cluster 1. Additionally, the expression of immune checkpoint genes (e.g., CD274, CTLA4, and PDCD1) was significantly higher in Cluster 2 (Fig. 3E), supporting the immune-suppressive tumor microenvironment characteristic of this subgroup.

Construction and validation of a prognostic model for ccRCC patients based on RHO-GTPase genes

We used LASSO regression to reduce the number of RHO-GTPase genes and construct a risk prognostic model. The optimal model was achieved when lambda = 0.056 (Fig. 4A). A total of 6 RHO-GTPase genes, including ARHGAP11B, CYFIP2, IQGAP2, NUF2, PLK1, and VAV3, were selected as prognostic features (Fig. 4B). The risk score formula is as follows:

$$\text{Risk score} = (0.066) \times \text{ARHGAP11B} + (-0.1678) \times \text{CYFIP2} + (-0.2203) \times \text{IQGAP2} + (0.0537) \times \text{NUF2} + (0.2872) \times \text{PLK1} + (-0.0666) \times \text{VAV3}.$$

Using the median risk score (Fig. 4C), ccRCC patients were classified into high-risk and low-risk groups. As the risk score increased, patients' survival duration decreased and mortality increased. The gene expression heatmap showed that the expression of CYFIP2, IQGAP2, and VAV3 decreased significantly with higher risk scores, suggesting these are protective genes, while the expression of ARHGAP11B, NUF2, and PLK1 increased with higher risk scores, suggesting they are risk genes (Fig. 4C). Kaplan–Meier survival analysis revealed that patients in the high-risk group had significantly worse prognosis than those in the low-risk group. The cumulative probability curve showed that the high-risk group had a significantly higher cumulative risk of adverse outcomes (such as death or disease recurrence) over 10 years compared to the low-risk group (Fig. 4D). Additionally, the survival ROC curves and their AUC values at 1-year, 3-year, and 5-year were all above 0.7, indicating the strong predictive ability of this model (Fig. 4E). We validated the model using 39 independent ccRCC patients from the GEO database. The results showed significant survival differences between the high-risk and low-risk groups (Fig. 4F), and the AUC values for 1-year, 3-year, and 5-year survival were all above 0.7 (Fig. 4G), suggesting that the model has robust predictive capacity.

Comparison of clinical nomogram and prognostic model performance based on RHO-GTPase model genes

Univariate Cox regression analysis revealed that six RHO-GTPase model genes, along with TNM staging, were significantly associated with prognosis (Fig. 5A). After performing multivariate Cox regression analysis, we identified IQGAP2 and TNM stage as independent prognostic factors (Fig. 5B). We incorporated these six RHO-GTPase model genes and TNM stage into the development of a clinical nomogram, which can provide guidance for clinical prognosis. The nomogram we developed predicts the overall survival (OS) of ccRCC patients at 1, 2, 3, 4, and 5 years, with a C-index of 0.774, indicating strong predictive performance (Fig. 5C). The calibration curve suggests that the nomogram closely follows the ideal curve, indicating accurate predictions (Fig. 5D). Decision curve analysis (DCA) shows that the clinical prognostic model based on the RHO-GTPase model genes significantly outperforms several other clinical prognostic models [15–18], demonstrating high clinical value (Fig. 5E).

High RHO-GTPase risk patients are associated with an immunosuppressive microenvironment

We utilized six different immune algorithms to analyze immune cell correlations in different risk groups. Figure 6A shows that high-risk ccRCC patients exhibit a more active immune microenvironment. Specifically, levels of tumor-associated immune cells, such as endothelial cells (Fig. 6B), CD4 + T cells (Fig. 6C), and NK cells (Fig. 6D), were higher in the low RHO-GTPase risk group. Conversely, Treg cells (Fig. 6E), activated myeloid dendritic cells (Fig. 6F), CD4 + Th1 T cells (Fig. 6G), cancer-associated fibroblasts (Fig. 6H), and CD4 + Th2

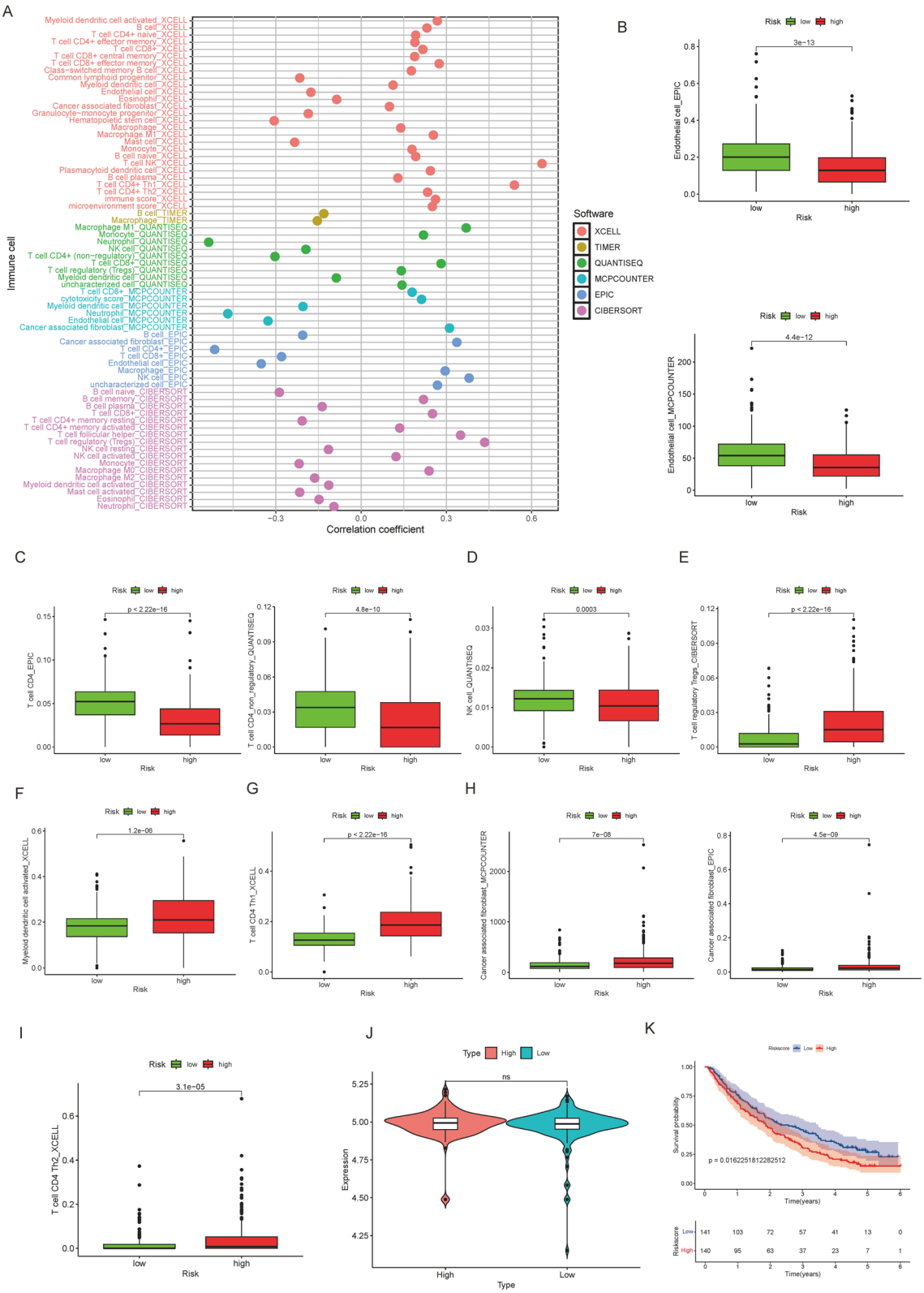

T cells (Fig. 6I) were more abundant in the high RHO-GTPase risk group. These findings suggest that high-risk RHO-GTPase ccRCC patients have a significantly more immunosuppressive tumor microenvironment. To

◂**Fig. 6** Differences in immune cells between RHO-GTPase risk groups. **A** Differences in immune cells across sample groups as observed by six different immune algorithms (TIMER, xCell, MCP-counter, CIBERSORT, EPIC, and quanTIseq). The x-axis represents the correlation coefficient, and the y-axis shows immune cell components with significantly different expression across algorithms. **B** Endothelial cells, **C** CD4 + T cells, **D** NK cells were more abundant in the low RHO-GTPase risk group. **E** Treg cells, **F** activated myeloid dendritic cells, **G** CD4 + Th1 T cells, **H** cancer-associated fibroblasts, and **I** CD4 + Th2 T cells were more abundant in the high RHO-GTPase risk group. **J** PD-1 gene expression in the anti-PD-1 immunotherapy dataset was higher in the low-risk group. **K** Kaplan–Meier (KM) survival curves showing the effectiveness of the RHO-GTPase prognostic model in stratifying risk for immune therapy patients

investigate whether RHO-GTPase risk scores could predict the efficacy of immune therapy in ccRCC, we analyzed PD-1 gene expression in an anti-PD-1 immunotherapy dataset. We found that PD-1 expression was higher in the low-risk group compared to the high-risk group (Fig. 6J). Kaplan–Meier (KM) survival curves indicated significant differences between the high and low RHO-GTPase risk groups (Fig. 6K), suggesting that the RHO-GTPase risk model is effective in stratifying risk for immune therapy patients.

RHO-GTPase gene scoring for chemotherapy drug sensitivity prediction in ccRCC patients

To assess the response of different risk ccRCC samples to treatment, we utilized the largest publicly available pharmacogenomic database, the Genomics of Drug Sensitivity in Cancer (GDSC), and predicted each sample's response to drug treatments based on their transcriptomic data. The results showed that the IC50 values of 107 drugs significantly differed between high and low-risk patients (Fig. 7A). High-risk patients had significantly lower IC50 values for drugs like CGP.60474, VX.680, vinblastine, parthenolide, and KU.55933, suggesting these drugs might be more effective and sensitive for high-risk patients (Fig. 7B). In contrast, FH535, AKT.inhibitor.VIII, GW.441756, BMS.708163, and AS601245 were among the top five most sensitive chemotherapy drugs for the low-risk group (Fig. 7C). Our findings provide valuable insights for chemotherapy drug selection in ccRCC patients.

Identification of potential drug targets for RHO-GTPase model genes in ccRCC patients

We further analyzed the potential of six RHO-GTPase model genes as diagnostic and therapeutic targets for ccRCC patients. By examining the expression levels of these genes in ccRCC tumor tissues and adjacent normal tissues from the TCGA database, we found that ARHGAP11B, NUF2, and PLK1 were overexpressed in ccRCC, while CYFIP2, IQGAP2, and VAV3 were underexpressed. These findings are consistent with our previous results, where ARHGAP11B, NUF2, and PLK1 were identified as risk genes, and CYFIP2, IQGAP2, and VAV3 as protective genes. Using single-cell RNA-sequencing analysis, we examined the expression of these genes in different cell subpopulations within ccRCC patients. Figure 8B shows the distribution of major cell subpopulations in ccRCC patients. Specifically, ARHGAP11B, NUF2, and PLK1 were predominantly expressed in proliferating T cells, while VAV3 was mainly expressed in endothelial cells. CYFIP2 and IQGAP2 were expressed in various immune cell types (Fig. 8C), suggesting their involvement in immune activity. We further validated the expression patterns of the six RHO-GTPase model genes at the cell line level using the Cancer Cell Line Encyclopedia (CCLE) dataset. Gene expression data from ccRCC cell lines [19] (OSRC2, 786-O, 769-P, Caki-2, A-498, and ACHN) and the normal renal epithelial cell line HEK TE were retrieved from the DepMap portal [20]. As shown in Supplementary Fig. 1, IQGAP2 exhibited significantly higher expression in normal HK2 cells compared to ccRCC cell lines, consistent with our tissue-level findings. CYFIP2 and VAV3 were expressed at lower levels in normal cells relative to most ccRCC cell lines, while PLK1 and NUF2 showed no significant differential expression. Additionally, we validated the protein expression levels of RHO-GTPase model genes in normal and ccRCC patients using the HPA database (Fig. 8D). The inactivation of VHL is a hallmark feature of ccRCC, and its substrates are important therapeutic targets. We found that the six RHO-GTPase model genes were positively correlated with VHL expression in ccRCC patients, suggesting they may participate in the regulation of VHL.

Discussion

Clear cell renal cell carcinoma (ccRCC) is a major subtype of renal cell carcinoma, accounting for approximately 60–85% of cases [21]. A significant challenge in clinical practice is prognostic stratification of patients to optimize the benefits of targeted therapies. Currently, the most commonly used prognostic models are the Memorial Sloan Kettering Cancer Center (MSKCC) criteria [22] and the International Metastatic Renal Cell Carcinoma Database Consortium (IMDC) criteria [23]. However, these models focus primarily on clinical features and fail to integrate the genetic information of ccRCC, which could offer more precise prognostic insights. Identifying biomarkers for prognostic stratification is a promising approach, including grouping patients based on the prognosis related to tumor gene sets, such as TGF-β signaling [24]. Herein, we introduce a novel

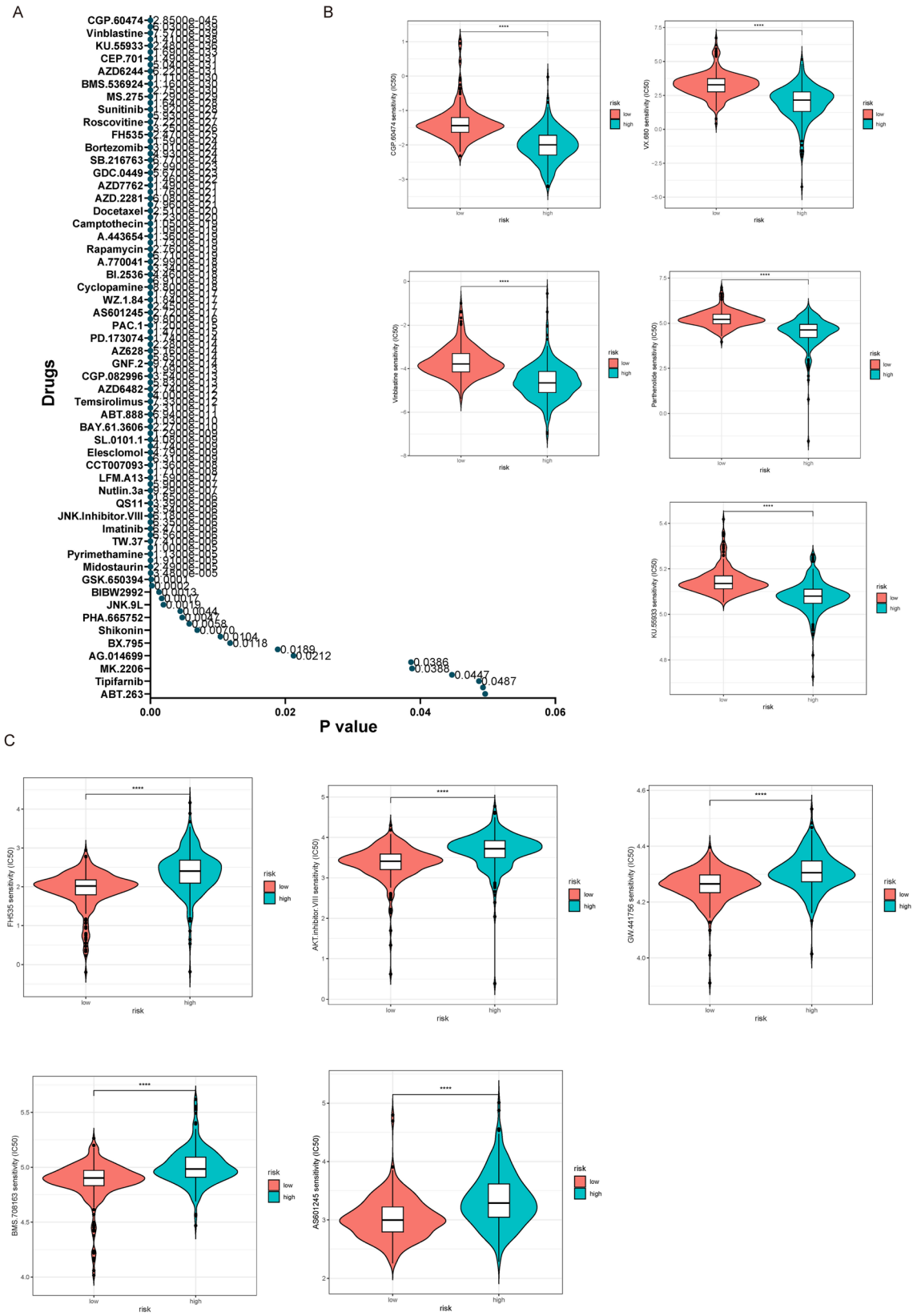

Fig. 7 Chemotherapy drug sensitivity prediction based on RHO-GTPase gene scoring in ccRCC patients. **A** IC50 values of 107 drugs differed significantly between high- and low-risk patients. **B** Top 5 chemotherapy drugs sensitive to high-risk patients. **C** Top 5 chemotherapy drugs sensitive to low-risk patients

prognostic pathway based on RHO-GTPase signaling genes for ccRCC. We analyzed the prognostic value, immune status, immune therapy potential, and chemotherapy drug sensitivity of RHO-GTPase signaling genes using a larger cohort of TCGA patients with diverse genetic backgrounds. Furthermore, we conducted gene, protein, and cellular-level identification of key RHO-GTPases, integrating them with clinical TNM staging to establish a nomogram aimed at improving the prognosis of ccRCC patients.

Our study unveiled several key findings. First, we performed molecular subtyping by extracting RHO-GTPase signaling genes and found that the activation of these genes is closely associated with ccRCC progression and poor prognosis. Functional enrichment analysis revealed that upregulated genes are involved in pathways like vascular smooth muscle contraction, cell adhesion molecules (CAMs), and the PI3K-Akt signaling pathway, all of which have been linked to tumor angiogenesis and enhanced invasion [25–27]. Further, KEGG pathway analysis confirmed that upregulated genes are significantly enriched in "Tryptophan metabolism," "Histidine metabolism," and other tumor-related pathways (e.g., PPAR signaling), suggesting that RHO-GTPase signaling may promote ccRCC progression through metabolic reprogramming [28, 29]. Moreover, immune microenvironment analysis revealed a significant enrichment of immunosuppressive cells (such as regulatory T cells) in RHO-GTPase-activated clusters [30], indicating that RHO-GTPase signaling may contribute to immune evasion by remodeling the immune microenvironment. Our findings suggest that the aberrant activation of RHO-GTPase signaling directly contributes to ccRCC's molecular pathology and indirectly accelerates tumor progression through metabolic regulation and immune microenvironment remodeling. This offers new insights into the mechanisms of RHO-GTPase signaling in ccRCC and lays the foundation for developing targeted therapies.

Secondly, we applied LASSO regression analysis and identified six key RHO-GTPase signaling genes—ARHGAP11B, NUF2, PLK1, CYFIP2, IQGAP2, and VAV3—as prognostic biomarkers for ccRCC. ccRCC is increasingly recognized as a metabolic disease characterized by extensive reprogramming of energy metabolism [31–34]. Notably, ccRCC cells exhibit partitioned metabolic flux through glycolysis [35–37], impaired mitochondrial bioenergetics and oxidative phosphorylation (OxPhos), as well as dysregulated lipid metabolism [35, 38–41]. These metabolic alterations play a crucial role in tumor progression, immune evasion, and therapy resistance. Interestingly, most of the six identified genes are known to regulate key metabolic pathways that are frequently altered in ccRCC, further supporting the biological relevance of our model. For example, IQGAP2 is involved in glycolysis/gluconeogenesis, glycogenolysis, and lipid metabolism [42], processes that are essential for ccRCC cell proliferation and adaptation to metabolic stress. ARHGAP11B localizes to mitochondria and promotes glutaminolysis, a crucial alternative energy pathway for cancer cells under metabolic stress [43]. PLK1 has been shown to regulate both glycolysis and the pentose phosphate pathway, influencing biosynthetic precursors necessary for rapid tumor growth [44]. These findings suggest that the RHO-GTPase signaling network may be intricately linked to the metabolic reprogramming of ccRCC, reinforcing the role of these genes as potential therapeutic targets. In this study, these genes were validated in independent datasets (TCGA and GSE29609) and effectively stratified patients into two risk groups with significantly different survival outcomes. Our prognostic model demonstrated robust predictive accuracy, with AUC values exceeding 0.7 for 1-year, 3-year, and 5-year survival in both training and validation cohorts. Additionally, decision curve analysis (DCA) confirmed that our model outperformed traditional clinical prognostic models [15–18]. To enhance clinical applicability, we further integrated these genes with clinical features to construct a nomogram, providing a comprehensive tool for individualized prognosis estimation in ccRCC.

Additionally, our study revealed the critical role of RHO-GTPase signaling in the ccRCC immune microenvironment using various immune algorithms, highlighting its dual value as both a tumor progression marker and a potential predictor of immune therapy response. We observed that low-risk patients had significantly higher levels of antitumor immune cells (e.g., CD4 + T cells, NK cells), suggesting a more effective immune surveillance and tumor clearance mechanism in these individuals [45, 46]. In contrast, high-risk patients had a significant enrichment of immunosuppressive cells (e.g., regulatory T cells, activated myeloid dendritic cells) and cancer-associated fibroblasts, reflecting strong immune evasion and a pro-tumor microenvironment [47, 48]. This stark contrast in immune cell distribution further elucidates the link between RHO-GTPase signaling and ccRCC immune microenvironment regulation.

Our study also demonstrated the potential application of RHO-GTPase risk scores in predicting sensitivity to immune therapy and chemotherapy. Low-risk patients showed higher PD-1 gene expression levels, correlating with better survival prognosis, suggesting that these patients may be more responsive to PD-1/PD-L1 immune checkpoint inhibitors. Kaplan–Meier survival analysis further validated the effectiveness of RHO-GTPase risk scores for patient stratification and prognostic assessment. Additionally, our drug sensitivity analysis, using the GDSC database, revealed significant differences in the IC50 values of 107 drugs between high- and low-risk groups. High-risk patients were more sensitive to drugs such as CGP.60474, VX.680, vinblastine, parthenolide, and KU.55933, while low-risk patients exhibited higher sensitivity to FH535, AKT inhibitors, GW.441756,

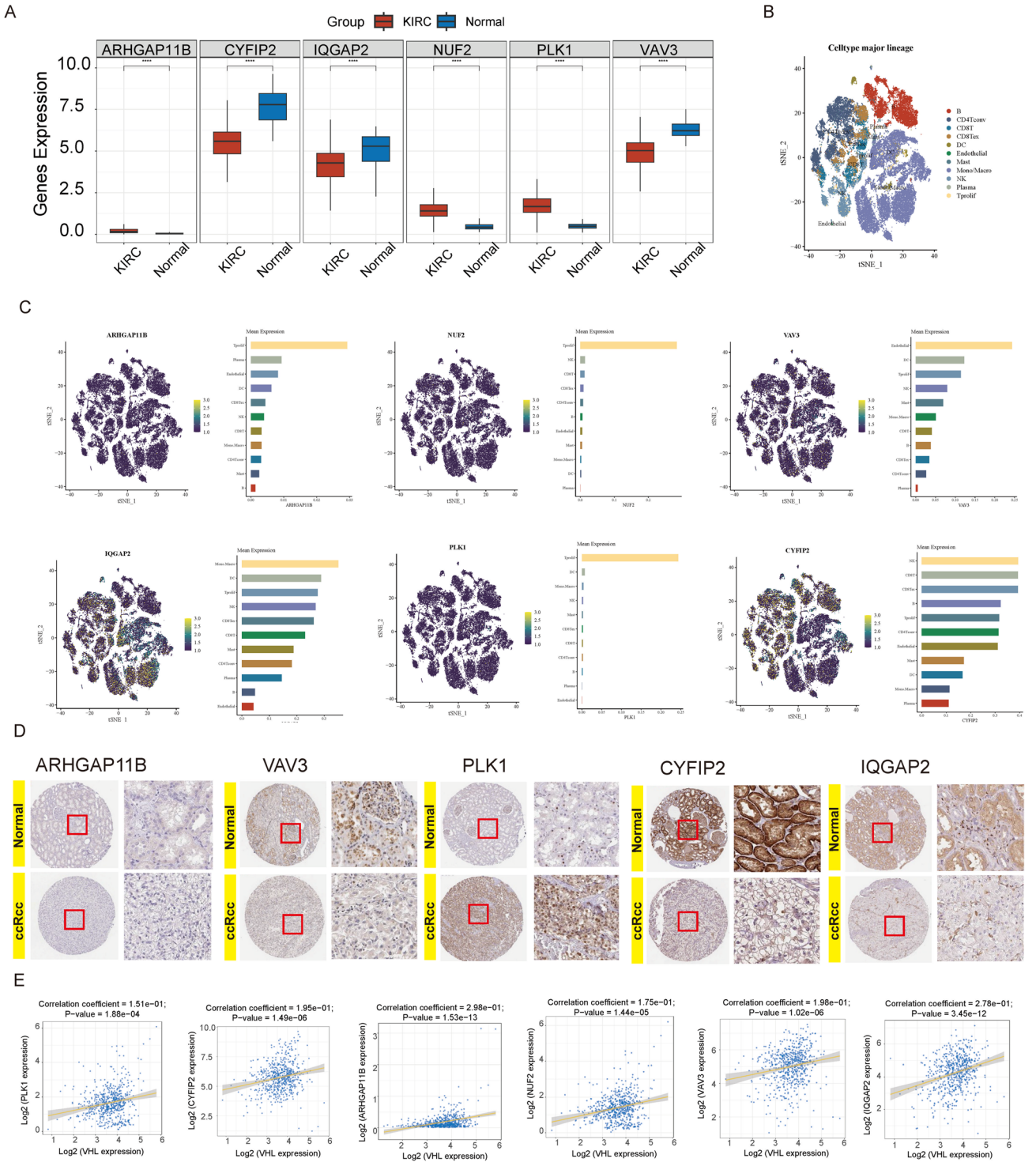

Fig. 8 Identifying potential drug targets for RHO-GTPase model genes in ccRCC patients. **A** Significant differences in the expression of six RHO-GTPase model genes between normal and ccRCC tissues from the TCGA database. **** represents $P < 0.0001$. **B** t-SNE plot of single-cell clustering from the GSE139555 dataset of ccRCC patients, with different colors representing different cell types. **C** Expression distribution of six RHO-GTPase model genes across different cell types in t-SNE plots and bar graphs showing expression abundance. Darker colors represent lower expression, while lighter colors indicate higher expression. **D** Protein expression levels of RHO-GTPase model genes in normal tissues and ccRCC patients. **E** Correlation map showing the relationship between six RHO-GTPase model genes and VHL expression

BMS.708163, and AS601245, offering potential therapeutic options for personalized treatment.

Lastly, we explored the expression and clinical relevance of the six RHO-GTPase model genes in ccRCC. Single-cell RNA-seq analysis showed that these genes exhibit specific expression patterns across different cell subpopulations. For example, ARHGAP11B, NUF2, and PLK1 are predominantly expressed in T cell proliferation, while VAV3 is highly expressed in endothelial cells, and CYFIP2 and IQGAP2 are widely distributed across various immune cells. Notably, the immune cell expression patterns of these protective genes suggest their key roles in regulating immune activity and maintaining the antitumor immune microenvironment. Validation using the HPA database showed that protein expression levels of these genes in normal tissues and ccRCC patients correlate with their transcriptional expression trends. This provides experimental support for studying the functional roles of these RHO-GTPase genes and their potential as protein biomarkers. Importantly, the positive correlation between the six RHO-GTPase genes and the VHL gene suggests that they may be involved in regulating the VHL pathway, a core molecular feature of ccRCC [49]. This implies that the RHO-GTPase model genes might influence the regulation of VHL substrates and contribute to ccRCC progression.

Our study has some limitations. Although we validated our prognostic stratification model in large cohort datasets, prospective validation in multicenter, large-scale cohorts are needed to enhance the model's applicability. Additionally, the molecular interactions between RHO-GTPase genes and immune status in ccRCC remain to be further explored. While we analyzed the expression, prognostic value, and potential mechanisms of the six RHO-GTPase genes, in vitro and in vivo validation of these pathways and mechanisms is still needed. Given the tissue and cell-type specificity of RHO-GTPase protein expression, future studies could provide new research directions for cancer treatment targeting RHO-GTPase signaling.

Conclusion

Our study developed a novel prognostic stratification biomarker—the RHO-GTPase signaling gene model, which can be used to assess clinical prognosis, immune status, immunotherapy response, and chemotherapy sensitivity in ccRCC patients, ultimately improving patient outcomes.

Supplementary Information The online version contains supplementary material available at https://doi.org/10.1007/s10238-025-01593-3.

Acknowledgements Figure 1A created with BioRender.com.

Author contributions K.H.G. and P.Y.M. analyzed and organized the data; Q.Y. and L.L.X. wrote and revised this manuscript; B.X.Z. generated the figure and tables. H.Z., Z.W.Z., and Z.W.Z. designed, revised, and supervised the study. All authors reviewed and approved the final manuscript.

Funding This work was supported by the Grants from Science and Technology Research Project of Henan Province (No. 222102310571), the National Natural Science Foundation of China (No.32200746), Guangzhou Science and Technology Program (No. 202201010873), and the Clinical Scientific Research Foundation of Guangdong Medical Association (No.2024HY-B5010).

Availability of data and materials No datasets were generated or analyzed during the current study.

Declarations

Conflict of interest The authors declare that they have no competing interests.

References

1. Young M, Jackson-Spence F, Beltran L, Day E, Suarez C, Bex A, Powles T, Szabados B. Renal cell carcinoma. Lancet. 2024;404(10451):476–91. https://doi.org/10.1016/S0140-6736(24)00917-6.
2. Hsieh JJ, Purdue MP, Signoretti S, Swanton C, Albiges L, Schmidinger M, Heng DY, Larkin J, Ficarra V. Renal cell carcinoma. Nat Rev Dis Primers. 2017;3:17009. https://doi.org/10.1038/nrdp.2017.9.
3. Verbiest A, Couchy G, Job S, Caruana L, Lerut E, Oyen R, de Reynies A, Tosco L, Joniau S, Van Poppel H, et al. Molecular subtypes of clear-cell renal cell carcinoma are prognostic for outcome after complete metastasectomy. Eur Urol. 2018;74(4):474–80. https://doi.org/10.1016/j.eururo.2018.01.042.
4. Geynisman DM, Plimack ER. Systemic therapy for advanced non-clear-cell renal cell carcinoma: slow but definite progress. Eur Urol. 2021;80(2):171–3. https://doi.org/10.1016/j.eururo.2021.04.031.
5. Neuzillet Y, Tillou X, Mathieu R, Long JA, Gigante M, Paparel P, Poissonnier L, Baumert H, Escudier B, Lang H, et al. Renal cell carcinoma (RCC) in patients with end-stage renal disease

exhibits many favourable clinical, pathologic, and outcome features compared with RCC in the general population. Eur Urol. 2011;60(2):366–73. https://doi.org/10.1016/j.eururo.2011.02.035.
6. Sun M, Shariat SF, Cheng C, Ficarra V, Murai M, Oudard S, Pantuck AJ, Zigeuner R, Karakiewicz PI. Prognostic factors and predictive models in renal cell carcinoma: a contemporary review. Eur Urol. 2011;60(4):644–61. https://doi.org/10.1016/j.eururo.2011.06.041.
7. Van Poppel H, Becker F, Cadeddu JA, Gill IS, Janetschek G, Jewett MA, Laguna MP, Marberger M, Montorsi F, Polascik TJ, et al. Treatment of localised renal cell carcinoma. Eur Urol. 2011;60(4):662–72. https://doi.org/10.1016/j.eururo.2011.06.040.
8. Wang J, Yin X, He W, Xue W, Zhang J, Huang Y. SUV39H1 deficiency suppresses clear cell renal cell carcinoma growth by inducing ferroptosis. Acta Pharm Sin B. 2021;11(2):406–19. https://doi.org/10.1016/j.apsb.2020.09.015.
9. Stewart GD, O'Mahony FC, Powles T, Riddick AC, Harrison DJ, Faratian D. What can molecular pathology contribute to the management of renal cell carcinoma? Nat Rev Urol. 2011;8(5):255–65. https://doi.org/10.1038/nrurol.2011.43.
10. Yang Q, Zhuo Z, Qiu X, Luo R, Guo K, Wu H, Jiang R, Li J, Lian Q, Chen P, et al. Adverse clinical outcomes and immunosuppressive microenvironment of RHO-GTPase activation pattern in hepatocellular carcinoma. J Transl Med. 2024;22(1):122. https://doi.org/10.1186/s12967-024-04926-0.
11. Jansen S, Gosens R, Wieland T, Schmidt M. Paving the Rho in cancer metastasis: Rho GTPases and beyond. Pharmacol Ther. 2018;183:1–21. https://doi.org/10.1016/j.pharmthera.2017.09.002.
12. Shen C, Kaelin WG Jr. The VHL/HIF axis in clear cell renal carcinoma. Semin Cancer Biol. 2013;23(1):18–25. https://doi.org/10.1016/j.semcancer.2012.06.001.
13. Akhtar M, Al-Bozom IA, Al Hussain T. Molecular and metabolic basis of clear cell carcinoma of the kidney. Adv Anat Pathol. 2018;25(3):189–96. https://doi.org/10.1097/PAP.0000000000000185.
14. Braun DA, Hou Y, Bakouny Z, Ficial M, Sant' Angelo M, Forman J, Ross-Macdonald P, Berger AC, Jegede OA, Elagina L, et al. Interplay of somatic alterations and immune infiltration modulates response to PD-1 blockade in advanced clear cell renal cell carcinoma. Nat Med. 2020;26(6):909–18. https://doi.org/10.1038/s41591-020-0839-y.
15. Ye Y, Zeng S, Hu X. Unveiling the hidden role of disulfidptosis in kidney renal clear cell carcinoma: a prognostic signature for personalized treatment. Apoptosis. 2024;29(5–6):693–708. https://doi.org/10.1007/s10495-023-01933-2.
16. Sun Z, Tao W, Guo X, Jing C, Zhang M, Wang Z, Kong F, Suo N, Jiang S, Wang H. Construction of a lactate-related prognostic signature for predicting prognosis, tumor microenvironment, and immune response in kidney renal clear cell carcinoma. Front Immunol. 2022;13: 818984. https://doi.org/10.3389/fimmu.2022.818984.
17. Chen H, Pan Y, Jin X, Chen G. Identification of a Four hypoxia-associated long non-coding RNA signature and establishment of a nomogram predicting prognosis of clear cell renal cell carcinoma. Front Oncol. 2021;11: 713346. https://doi.org/10.3389/fonc.2021.713346.
18. Luo G, Wang L, Zheng Z, Gao B, Lei C. Cuproptosis-Related Ferroptosis genes for Predicting Prognosis in kidney renal clear cell carcinoma. Eur J Med Res. 2023;28(1):176. https://doi.org/10.1186/s40001-023-01137-z.
19. Xu Y, Li L, Yang W, Zhang K, Zhang Z, Yu C, Qiu J, Cai L, Gong Y, Zhang Z, et al. TRAF2 promotes M2-polarized tumor-associated macrophage infiltration, angiogenesis and cancer progression by inhibiting autophagy in clear cell renal cell carcinoma. J Exp Clin Cancer Res. 2023;42(1):159. https://doi.org/10.1186/s13046-023-02742-w.
20. Ghandi M, Huang FW, Jane-Valbuena J, Kryukov GV, Lo CC, McDonald ER 3rd, Barretina J, Gelfand ET, Bielski CM, Li H, et al. Next-generation characterization of the Cancer Cell Line Encyclopedia. Nature. 2019;569(7757):503–8. https://doi.org/10.1038/s41586-019-1186-3.
21. Mitchell TJ, Turajlic S, Rowan A, Nicol D, Farmery JHR, O'Brien T, Martincorena I, Tarpey P, Angelopoulos N, Yates LR, et al. Timing the landmark events in the evolution of clear cell renal cell cancer: TRACERx renal. Cell. 2018;173(3):611–23. https://doi.org/10.1016/j.cell.2018.02.020.
22. Mekhail TM, Abou-Jawde RM, Boumerhi G, Malhi S, Wood L, Elson P, Bukowski R. Validation and extension of the Memorial Sloan-Kettering prognostic factors model for survival in patients with previously untreated metastatic renal cell carcinoma. J Clin Oncol. 2005;23(4):832–41. https://doi.org/10.1200/JCO.2005.05.179.
23. Perez-Valderrama B, Arranz Arija JA, Rodriguez Sanchez A, Pinto Marin A, Borrega Garcia P, Castellano Gaunas DE, Rubio Romero G, Maximiano Alonso C, Villa Guzman JC, Puertas Alvarez JL, et al. Validation of the International Metastatic Renal-Cell Carcinoma Database Consortium (IMDC) prognostic model for first-line pazopanib in metastatic renal carcinoma: the Spanish Oncologic Genitourinary Group (SOGUG) SPAZO study. Ann Oncol. 2016;27(4):706–11. https://doi.org/10.1093/annonc/mdv601.
24. Boguslawska J, Kedzierska H, Poplawski P, Rybicka B, Tanski Z, Piekielko-Witkowska A. Expression of genes involved in cellular adhesion and extracellular matrix remodeling correlates with poor survival of patients with renal cancer. J Urol. 2016;195(6):1892–902. https://doi.org/10.1016/j.juro.2015.11.050.
25. Hoff PM, Machado KK. Role of angiogenesis in the pathogenesis of cancer. Cancer Treat Rev. 2012;38(7):825–33. https://doi.org/10.1016/j.ctrv.2012.04.006.
26. Morgado M, Cairrao E, Santos-Silva AJ, Verde I. Cyclic nucleotide-dependent relaxation pathways in vascular smooth muscle. Cell Mol Life Sci. 2012;69(2):247–66. https://doi.org/10.1007/s00018-011-0815-2.
27. Karar J, Maity A. PI3K/AKT/mTOR pathway in angiogenesis. Front Mol Neurosci. 2011;4:51. https://doi.org/10.3389/fnmol.2011.00051.
28. Tanaka M, Toth F, Polyak H, Szabo A, Mandi Y, Vecsei L. Immune influencers in action: metabolites and enzymes of the tryptophan-kynurenine metabolic pathway. Biomedicines. 2021. https://doi.org/10.3390/biomedicines9070734.
29. Campos B, Rivetti C, Tauler R, Pina B, Barata C. Tryptophan hydroxylase (TRH) loss of function mutations in Daphnia deregulated growth, energetic, serotoninergic and arachidonic acid metabolic signalling pathways. Sci Rep. 2019;9(1):3693. https://doi.org/10.1038/s41598-019-39987-5.
30. Burbage M, Keppler SJ, Montaner B, Mattila PK, Batista FD. The small rho GTPase TC10 modulates B cell immune responses. J Immunol. 2017;199(5):1682–95. https://doi.org/10.4049/jimmunol.1602167.
31. di Meo NA, Lasorsa F, Rutigliano M, Milella M, Ferro M, Battaglia M, Ditonno P, Lucarelli G. The dark side of lipid metabolism in prostate and renal carcinoma: novel insights into molecular diagnostic and biomarker discovery. Expert Rev Mol Diagn. 2023;23(4):297–313. https://doi.org/10.1080/14737159.2023.2195553.
32. Lucarelli G, Loizzo D, Franzin R, Battaglia S, Ferro M, Cantiello F, Castellano G, Bettocchi C, Ditonno P, Battaglia M. Metabolomic insights into pathophysiological mechanisms and biomarker discovery in clear cell renal cell carcinoma. Expert Rev Mol

Diagn. 2019;19(5):397–407. https://doi.org/10.1080/14737159.2019.1607729.
33. di Meo NA, Lasorsa F, Rutigliano M, Loizzo D, Ferro M, Stella A, Bizzoca C, Vincenti L, Pandolfo SD, Autorino R, et al. Renal cell carcinoma as a metabolic disease: an update on main pathways, potential biomarkers, and therapeutic targets. Int J Mol Sci. 2022. https://doi.org/10.3390/ijms232214360.
34. De Marco S, Torsello B, Minutiello E, Morabito I, Grasselli C, Bombelli S, Zucchini N, Lucarelli G, Strada G, Perego RA, et al. The cross-talk between Abl2 tyrosine kinase and TGFbeta1 signalling modulates the invasion of clear cell Renal Cell Carcinoma cells. FEBS Lett. 2023;597(8):1098–113. https://doi.org/10.1002/1873-3468.14531.
35. Bianchi C, Meregalli C, Bombelli S, Di Stefano V, Salerno F, Torsello B, De Marco S, Bovo G, Cifola I, Mangano E, et al. The glucose and lipid metabolism reprogramming is grade-dependent in clear cell renal cell carcinoma primary cultures and is targetable to modulate cell viability and proliferation. Oncotarget. 2017;8(69):113502–15. https://doi.org/10.18632/oncotarget.23056.
36. Ragone R, Sallustio F, Piccinonna S, Rutigliano M, Vanessa G, Palazzo S, Lucarelli G, Ditonno P, Battaglia M, Fanizzi FP, et al. Renal cell carcinoma: a study through NMR-based metabolomics combined with transcriptomics. Diseases. 2016. https://doi.org/10.3390/diseases4010007.
37. Lucarelli G, Galleggiante V, Rutigliano M, Sanguedolce F, Cagiano S, Bufo P, Lastilla G, Maiorano E, Ribatti D, Giglio A, et al. Metabolomic profile of glycolysis and the pentose phosphate pathway identifies the central role of glucose-6-phosphate dehydrogenase in clear cell-renal cell carcinoma. Oncotarget. 2015;6(15):13371–86. https://doi.org/10.18632/oncotarget.3823.
38. Lucarelli G, Rutigliano M, Sallustio F, Ribatti D, Giglio A, Lepore Signorile M, Grossi V, Sanese P, Napoli A, Maiorano E, et al. Integrated multi-omics characterization reveals a distinctive metabolic signature and the role of NDUFA4L2 in promoting angiogenesis, chemoresistance, and mitochondrial dysfunction in clear cell renal cell carcinoma. Aging (Albany NY). 2018;10(12):3957–85. https://doi.org/10.18632/aging.101685.
39. Bombelli S, Torsello B, De Marco S, Lucarelli G, Cifola I, Grasselli C, Strada G, Bovo G, Perego RA, Bianchi C. 36-kDa annexin A3 isoform negatively modulates lipid storage in clear cell renal cell carcinoma cells. Am J Pathol. 2020;190(11):2317–26. https://doi.org/10.1016/j.ajpath.2020.08.008.
40. Lucarelli G, Rutigliano M, Loizzo D, di Meo NA, Lasorsa F, Mastropasqua M, Maiorano E, Bizzoca C, Vincenti L, Battaglia M, et al. MUC1 tissue expression and its soluble form CA15–3 identify a clear cell renal cell carcinoma with distinct metabolic profile and poor clinical outcome. Int J Mol Sci. 2022. https://doi.org/10.3390/ijms232213968.
41. Milella M, Rutigliano M, Lasorsa F, Ferro M, Bianchi R, Fallara G, Crocetto F, Pandolfo SD, Barone B, d'Amati A, et al. The role of MUC1 in renal cell carcinoma. Biomolecules. 2024. https://doi.org/10.3390/biom14030315.
42. Vaitheesvaran B, Hartil K, Navare A, Zheng POB, Golden A. Role of the tumor suppressor IQGAP2 in metabolic homeostasis: possible link between diabetes and cancer. Metabolomics. 2014;10(5):920–37. https://doi.org/10.1007/s11306-014-0639-9.
43. Xing L, Gkini V, Nieminen AI, Zhou HC, Aquilino M, Naumann R, Reppe K, Tanaka K, Carmeliet P, Heikinheimo O, et al. Functional synergy of a human-specific and an ape-specific metabolic regulator in human neocortex development. Nat Commun. 2024;15(1):3468. https://doi.org/10.1038/s41467-024-47437-8.
44. Gutteridge RE, Singh CK, Ndiaye MA, Ahmad N. Targeted knockdown of polo-like kinase 1 alters metabolic regulation in melanoma. Cancer Lett. 2017;394:13–21. https://doi.org/10.1016/j.canlet.2017.02.013.
45. Lee SW, Park HJ, Kim N, Hong S. Natural killer dendritic cells enhance immune responses elicited by alpha -galactosylceramide-stimulated natural killer T cells. Biomed Res Int. 2013;2013:460706. https://doi.org/10.1155/2013/460706.
46. Stern C, Kasnitz N, Kocijancic D, Trittel S, Riese P, Guzman CA, Leschner S, Weiss S. Induction of CD4(+) and CD8(+) anti-tumor effector T cell responses by bacteria mediated tumor therapy. Int J Cancer. 2015;137(8):2019–28. https://doi.org/10.1002/ijc.29567.
47. Diederich D, Yang ZH, Buhler FR, Luscher TF. Impaired endothelium-dependent relaxations in hypertensive resistance arteries involve cyclooxygenase pathway. Am J Physiol. 1990;258(2 Pt 2):H445-451. https://doi.org/10.1152/ajpheart.1990.258.2.H445.
48. Iglesias-Escudero M, Arias-Gonzalez N, Martinez-Caceres E. Regulatory cells and the effect of cancer immunotherapy. Mol Cancer. 2023;22(1):26. https://doi.org/10.1186/s12943-023-01714-0.
49. Vanharanta S, Shu W, Brenet F, Hakimi AA, Heguy A, Viale A, Reuter VE, Hsieh JJ, Scandura JM, Massague J. Epigenetic expansion of VHL-HIF signal output drives multiorgan metastasis in renal cancer. Nat Med. 2013;19(1):50–6. https://doi.org/10.1038/nm.3029.